Eur. Phys. J. D (2022) 76:249
https://doi.org/10.1140/epjd/s10053-022-00572-7

THE EUROPEAN PHYSICAL JOURNAL D

Regular Article – Ultraintense and Ultrashort Laser Fields

Analysis of the asymmetry of Autler–Townes doublets in the energy spectra of photoelectrons produced at two-photon ionization of atoms by strong laser pulses

A. Bunjac[a], D. B. Popović[b], and N. S. Simonović[c]

Institute of Physics, University of Belgrade, Pregrevica 118, 11080 Belgrade, Serbia

Received 1 November 2022 / Accepted 29 November 2022 / Published online 21 December 2022

Abstract. We analyzed the asymmetry of Autler–Townes doublets in the calculated photoelectron energy spectra for the two-photon ionization of the hydrogen atom by an intense short laser pulse that resonantly couples its ground state with the excited 2p state. The spectra are calculated applying the method of time-dependent amplitudes using two approaches of different level of approximation. The first approach involves solving a complete set of equations for amplitudes, which, in addition to amplitudes of coupled (1s, 2p) and continuous states, also includes the amplitudes of other discrete (nonessential) states. The second approach is the three-level model that includes only the amplitudes of the two coupled states and those of continuum states. By comparing the spectra obtained using these two approaches it is confirmed that the shift of the Autler–Townes doublets, which exists only in the spectra obtained by solving the full set of equations, can be attributed to the AC Stark shift, which is a consequence of the coupling with nonessential states. Finally, it was found that the asymmetry in the intensity of the Autler–Townes doublet components, which appears in the spectra obtained using both computational approaches, is primarily due to the decrease in the transition probability between the 2p and continuum states with increasing photoelectron energy.

1 Introduction

Multiphoton ionization of an atom by a laser field that resonantly couples its ground state to an excited state can serve as a probe for the field induced Rabi dynamics of the coupled states. In the time-dependent picture this dynamics is manifested as the periodic transfer of population from one state to another—the so-called Rabi flopping (see e.g. [1]), but in the frequency domain it leads to a splitting of the resonant peak in the photoabsorption spectrum, known as the Autler–Townes (AT) doublet. Before the availability of coherent light sources this splitting was first detected in the absorption spectrum of a molecule using radiation from the radio frequency domain [2].

Apart from the photoabsorption spectra, the AT splitting can also be detected in the energy spectra of photoelectrons produced at multiphoton ionization of atoms and molecules. However, despite theoretical predictions to observe it at short wavelengths [3–8], its direct observation at XUV wavelengths has been reported only recently, after the free-electron lasers with high temporal and spatial coherence became available [9]. Applying intense pulses from such a source, one-photon Rabi oscillations are successfully induced between the ground state and an excited state of the atom, particularly if the carrier frequency of the source is resonant for the transition between these states. A second photon from the same pulse can further ionize the atom from the excited state, so finally we have resonant two-photon ionization. The emitted photoelectrons coherently probe the dynamics of the coupled states and the photoelectron energy spectrum (PES) reveals the AT doublet.

A detailed theoretical analysis of the AT splitting, instead of a simple doublet, predicts a multiple-peak pattern in the PES [5–8], as well as additional effects such as energy shift and asymmetry of the pattern [3,4,7,8]. An explanation for the multiple-peak structure, which has been proposed in previous studies [6], is the so-called dynamic interference of photoelectrons emitted on the rising and falling sides of the pulse with a time delay. However, subsequent analysis has shown that this explanation is not adequate in the general case [10,11], which is also confirmed by our recent calculations [12].

In this paper, we focus on the analysis of shift and asymmetry of AT doublets, taking as an example the resonant two-photon ionization of hydrogen atoms by short laser pulses. In order to get more pronounced

[a] e-mail: bunjac@ipb.ac.rs
[b] e-mail: duska@ipb.ac.rs
[c] e-mail: simonovic@ipb.ac.rs (corresponding author)

effects, we have chosen pulses of higher intensity and shorter duration than previously used. In the next section we present two computational approaches with different degrees of approximation for calculating the populations of atomic states and the photoelectron energy spectra. Both approaches are based on the method of time-dependent amplitudes, whereby the first solves the full set of equations for amplitudes, while the second takes into account only two resonantly coupled states and continuum states. In Sect. 3 we present the results obtained within these approaches and analyze the above effects in the AT splitting. A summary and conclusions are given in Sect. 4.

2 Model and computational approaches

The populations of atomic states during the interaction of the atom with the laser pulse, including their final values when the pulse has expired, and the photoelectron energy spectra, that are the subject of the analysis carried out in the next section, were obtained by solving the time-dependent Schrödinger equation (in atomic units)

$$i\frac{\mathrm{d}}{\mathrm{d}t}|\psi(t)\rangle = (H_0 + z\mathcal{E}(t))|\psi(t)\rangle. \tag{1}$$

Here $|\psi(t)\rangle$ is the non-stationary atomic state at time t, H_0 is the Hamiltonian of the field-free (bare) atom, $\mathcal{E}(t)$ is the electric field component of the laser pulse and z is the projection of the electron-nucleus distance in the field direction. The term $z\,\mathcal{E}(t)$ describes the atom-field interaction in the dipole approximation using the length gauge. We consider a linearly polarized laser pulse whose electric field component reads

$$\mathcal{E}(t) = \mathcal{E}_0\, g(t) \cos\omega t, \tag{2}$$

where $\mathcal{E}_0$ is the peak value of the field strength, ω is the laser carrier frequency and the function $g(t)$ determines the shape of the pulse envelope.

Equation (1) is solved numerically assuming that the atom is initially in its ground state, i.e. $|\psi(t_0)\rangle = |1\mathrm{s}\rangle$, where t_0 is a time before the beginning of the interaction. Since the atom interacting with the field (2) has axial symmetry, the z-projection of the electron angular momentum l_z is a constant of motion and the magnetic quantum number m is a good quantum number. Thus, the state $|\psi(t)\rangle$ is at any time t characterized by the value $m = 0$, which characterizes the ground state of the bare atom. Unless otherwise stated, atomic units (a.u.) are used throughout the paper.

2.1 The full set of equations for amplitudes

The state of the hydrogen atom at time t interacting with a laser field can be written as the superposition of eigenstates of the commuting observables H_0, $\mathbf{l}^2$, and l_z

$$|\psi(t)\rangle = \sum_{n,l} c_{nl}(t)|nl\rangle + \int \sum_{l} c_{\varepsilon l}(t)|\varepsilon l\rangle\,\mathrm{d}\varepsilon, \tag{3}$$

where $c_{nl}(t)$ and $c_{\varepsilon l}(t)$ are the time-dependent amplitudes for the population of discrete and continuum eigenstates, $|nl\rangle \equiv |nlm\rangle$ and $|\varepsilon l\rangle \equiv |\varepsilon lm\rangle$ with $m = 0$, respectively.

By substituting expansion (3) in Schrödinger equation (1) and projecting the result onto each eigenstate, one obtains the following set of equations for the amplitudes

$$\begin{aligned}
i\dot{c}_{nl} &= E_n\, c_{nl}(t) + \mathcal{E}(t)\sum_{n',l'}\langle nl|z|n'l'\rangle\, c_{n'l'}(t) \\
&\quad + \mathcal{E}(t)\int\sum_{l'}\langle nl|z|\varepsilon l'\rangle\, c_{\varepsilon l'}(t)\,\mathrm{d}\varepsilon, \\
i\dot{c}_{\varepsilon l} &= \varepsilon\, c_{\varepsilon l}(t) + \mathcal{E}(t)\sum_{n',l'}\langle \varepsilon l|z|n'l'\rangle\, c_{n'l'}(t) \\
&\quad + \mathcal{E}(t)\int\sum_{l'}\langle \varepsilon l|z|\varepsilon' l'\rangle\, c_{\varepsilon' l'}(t)\,\mathrm{d}\varepsilon',
\end{aligned} \tag{4}$$

where E_n and ε are the values of the discrete and continuum energy levels of the bare atom, respectively.

By representing the integral over ε by the sum over a set of its discretized values ε_i and neglecting the continuum-continuum interaction, the set of integro-differential equations (4) reduces to the following set of differential equations

$$\begin{aligned}
i\dot{c}_{nl} &= E_n\, c_{nl}(t) + \mathcal{E}(t)\sum_{n',l'}\langle nl|z|n'l'\rangle\, c_{n'l'}(t) \\
&\quad + \mathcal{E}(t)\sum_{i,l'}\langle nl|z|\varepsilon_i l'\rangle\, c_{\varepsilon_i l'}(t)\,\Delta\varepsilon, \\
i\dot{c}_{\varepsilon_i l} &= \varepsilon\, c_{\varepsilon_i l}(t) + \mathcal{E}(t)\sum_{n',l'}\langle \varepsilon_i l|z|n'l'\rangle\, c_{n'l'}(t).
\end{aligned} \tag{5}$$

At the laser peak intensities up to few hundred TW/cm^2 that we consider here, in the expansion (3) it is sufficient to use the set of discrete states $|nl\rangle$ with $n \le 7$ and $l = 0, \ldots, n-1$, and s and d discretized continuum states (see Fig. 1) with energies in the interval from 5 to 8.6 eV with the step $\Delta\varepsilon = 0.01$ eV. The restriction to s and d continuum state justifies the neglect of the continuum-continuum interaction since the matrix elements between states of the same parity (here s and d) are equal to zero. The expressions for matrix elements $\langle nl|z|n'l'\rangle$ and $\langle nl|z|\varepsilon l'\rangle$ are given in Appendix A.

The quantities $|c_{nl}(t)|^2$ can be interpreted as the populations of atomic states $|nl\rangle$ after the interaction of the atom with the laser field which has ended at time t. Thus, the populations of states $|nl\rangle$, after time t_{ex} when we assume that the laser pulse has expired, are $|c_{nl}(t_{\mathrm{ex}})|^2$. Analogously, the quantity $|c_{\varepsilon l}(t_{\mathrm{ex}})|^2$ represents the probability density of finding the atomic elec-

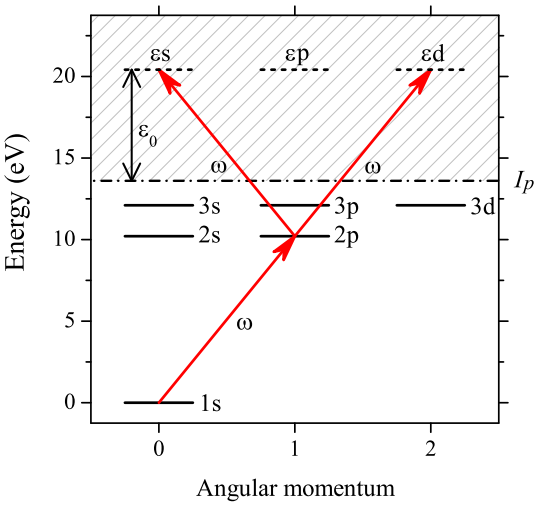

Fig. 1 Energy level scheme of the hydrogen atom and the two-photon absorption paths for transitions from the ground (1s) state to the final continuum states (εs and εd) via one-photon resonant excitation of 2p state

tron in the continuum state $|\varepsilon l\rangle$ after the pulse has expired.

Since the photoelectron yield at a given energy ε is proportional to the total probability density of finding the electron in continuum states corresponding to this energy, the photoelectron energy spectrum (PES) is adequately represented by the distribution

$$w(\varepsilon) = \sum_l |c_{\varepsilon l}(t_{\rm ex})|^2, \tag{6}$$

which in the considered case practically reduces to formula $w(\varepsilon) = |c_{\varepsilon \rm s}(t_{\rm ex})|^2 + |c_{\varepsilon \rm d}(t_{\rm ex})|^2$.

2.2 The three-level model

In the case of resonant or near resonant excitation of an intermediate state (here 2p), the other excited states are nonessential and at weak fields their role in the ionization process may be neglected, i.e. the process may be adequately described within the three-level model (E_1, E_2, ε) [6]. Then, the atomic state at time t reads

$$\begin{aligned}|\psi(t)\rangle = {} & C_{1\rm s}(t)|1\rm s\rangle + C_{2\rm p}(t)e^{-i\omega t}|2\rm p\rangle \\ & + e^{-2i\omega t}\int [C_{\varepsilon \rm s}(t)|\varepsilon \rm s\rangle + C_{\varepsilon \rm d}(t)|\varepsilon \rm d\rangle]\,\mathrm{d}\varepsilon, \end{aligned} \tag{7}$$

where $C_{1\rm s}(t)$, $C_{2\rm p}(t)$ and $C_{\varepsilon l}(t)$ are the time-dependent amplitudes for the population of states $|1\rm s\rangle$ (ground state), $|2\rm p\rangle$ (intermediate state) and $|\varepsilon l\rangle$, $l = 0, 2$ (continuum states), respectively. In this expansion the states $|2\rm p\rangle$ and $|\varepsilon l\rangle$ have been multiplied with the phase factors $e^{-i\omega t}$ and $e^{-2i\omega t}$ in order to simplify the set of equations for the amplitudes. By comparing Eqs. (3) and (7), one sees that $C_{1\rm s}(t) = c_{1\rm s}(t)$, $C_{2\rm p}(t) = e^{i\omega t}c_{2\rm p}(t)$ and $C_{\varepsilon l}(t) = e^{2i\omega t}c_{\varepsilon l}(t)$. Since the difference between the C and c sets of amplitudes is only in the phase factors, both sets adequately determine the populations of atomic states and photoelectron yield.

If we set the ground state energy to zero ($E_1 = 0$, as shown in Fig. 1), by inserting Eq. (7) in the Schrödinger equation (1) and applying the rotating wave approximation [1], we obtain the following system of equations for the amplitudes

$$\begin{aligned} i\dot{C}_{1\rm s} &= \frac{1}{2}D^*\mathcal{E}_0\, g(t) C_{2\rm p}(t), \\ i\dot{C}_{2\rm p} &= \frac{1}{2}D\,\mathcal{E}_0\, g(t) C_{1\rm s}(t) + (E_2 - \omega)C_{2\rm p}(t) \\ &\quad + \frac{1}{2}\mathcal{E}_0\, g(t)\int [d^*_{\varepsilon \rm s}C_{\varepsilon \rm s}(t) + d^*_{\varepsilon \rm d}C_{\varepsilon \rm d}(t)]\,\mathrm{d}\varepsilon, \\ i\dot{C}_{\varepsilon \rm s} &= \frac{1}{2}d_{\varepsilon \rm s}\,\mathcal{E}_0 g(t) C_{2\rm p}(t) + (I_p + \varepsilon - 2\omega)C_{\varepsilon \rm s}(t), \\ i\dot{C}_{\varepsilon \rm d} &= \frac{1}{2}d_{\varepsilon \rm d}\,\mathcal{E}_0 g(t) C_{2\rm p}(t) + (I_p + \varepsilon - 2\omega)C_{\varepsilon \rm d}(t). \end{aligned} \tag{8}$$

Note that, by taking $E_1 = 0$, the energies of the 2p and final continuum states are $E_2 = 0.375\,\text{a.u.} = 10.204\,\text{eV}$ and $I_p + \varepsilon$, respectively, where $I_p = 0.5\,\text{a.u.} = 13.606\,\text{eV}$ is the ionization potential of the hydrogen atom. Here $D = \langle 2\rm p|z|1\rm s\rangle$ and $d_{\varepsilon l} = \langle \varepsilon l|z|2\rm p\rangle$ are the dipole transition matrix elements for the excitation of the 2p state and for its subsequent ionization, respectively.

Using formal solutions of the third and fourth of Eq. (8)

$$C_{\varepsilon l}(t) = -\frac{i}{2}\mathcal{E}_0\, d_{\varepsilon l}\int_{-\infty}^{t} e^{-i(I_p+\varepsilon-2\omega)(t-t')} g(t')\, C_{2\rm p}(t')\,\mathrm{d}t', \tag{9}$$

where $l = 0, 2$, and the local approximation which assumes that the main contribution of the integral over t' stems from the times around $t' \sim t$ [13,14], the last term in the second of Eq. (8) reduces to

$$\begin{aligned} & \frac{1}{2}\mathcal{E}_0\, g(t)\int [d^*_{\varepsilon \rm s}C_{\varepsilon \rm s}(t) + d^*_{\varepsilon \rm d}C_{\varepsilon \rm d}(t)]\,\mathrm{d}\varepsilon \\ & \quad = -\pi i\,\frac{|d_{\varepsilon_0}|^2\mathcal{E}_0^2}{4}\, g^2(t)\, C_{2\rm p}(t), \end{aligned} \tag{10}$$

where $|d_{\varepsilon_0}|^2 = |d_{\varepsilon_0 \rm s}|^2 + |d_{\varepsilon_0 \rm d}|^2$ and $\varepsilon_0 = 2\omega - I_p$. Note also that the third and the forth of Eq. (8) are equivalent. Namely, dividing them by $d_{\varepsilon \rm s}$ and $d_{\varepsilon \rm d}$, respectively, they reduce to the same equation for the scaled amplitude $\tilde{C}_\varepsilon(t) = C_{\varepsilon \rm s}(t)/d_{\varepsilon \rm s} \equiv C_{\varepsilon \rm d}(t)/d_{\varepsilon \rm d}$ (which also follows from Eq. (9)).

Finally, one obtains the set of equations

$$\begin{aligned} i\dot{C}_{1\rm s} &= \frac{1}{2}\Omega_0^*\, g(t) C_{2\rm p}(t), \\ i\dot{C}_{2\rm p} &= \frac{1}{2}\Omega_0\, g(t) C_{1\rm s}(t) + \left[E_2 - \frac{i}{2}\Gamma g^2(t) - \omega\right] C_{2\rm p}(t), \end{aligned}$$

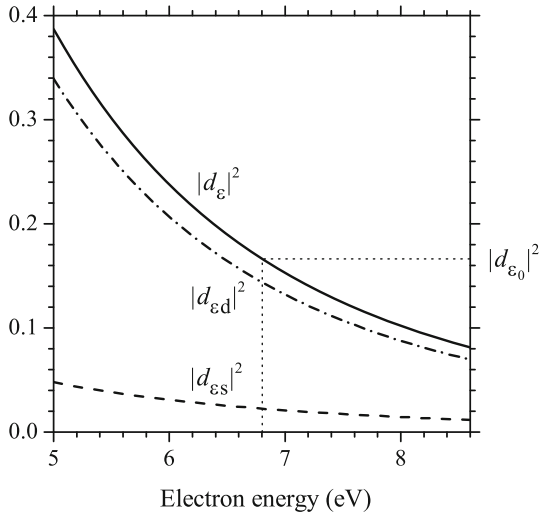

Fig. 2 The squares of modula of the dipole matrix elements for transitions from the 2p state to continuum states εs and εd (dashed and dash-dot lines, respectively), determined by Eq. (18), and their sum $|d_\varepsilon|^2$ (full line) in the energy interval $\varepsilon \in (6.4, 7.2)$ eV. The vertical and horizontal dotted lines mark the resonant energy $\varepsilon_0 = 6.803$ eV and the corresponding value of $|d_\varepsilon|^2$ ($|d_{\varepsilon_0}|^2 = 0.1663$ a.u.), respectively

$$i\dot{\tilde{C}}_\varepsilon = \frac{1}{2}\mathcal{E}_0 g(t) C_{2\mathrm{p}}(t) + (\varepsilon - \varepsilon_0)\tilde{C}_\varepsilon(t), \tag{11}$$

where $\Omega_0 = D\mathcal{E}_0$ is the frequency of Rabi flopping between the populations of states 1s and 2p at the peak value of laser intensity and

$$\Gamma = 2\pi \left| \frac{d_{\varepsilon_0}\mathcal{E}_0}{2} \right|^2 \tag{12}$$

is the ionization rate of the intermediate resonant state $|2\mathrm{p}\rangle$. The imaginary term $-\frac{i}{2}\Gamma g^2(t)$ describes the losses of the population of the intermediate state by the ionization into all final electron continuum states $|\varepsilon l\rangle$.

The PES can be determined applying formula (6), which here takes the form

$$w(\varepsilon) = |d_\varepsilon|^2 |\tilde{C}_\varepsilon(t_{\mathrm{ex}})|^2, \tag{13}$$

where $|d_\varepsilon|^2 = |d_{\varepsilon\mathrm{s}}|^2 + |d_{\varepsilon\mathrm{d}}|^2$. The values of the dipole matrix elements for transitions from the 1s to the 2p state and from the 2p state to continuum states are determined using Eqs. (17)–(21). The matrix element for the transition $1\mathrm{s} \to 2\mathrm{p}$ is $D = 0.7449$ a.u., while the values of $|d_\varepsilon|^2$ for $\varepsilon \in (5, 8.6)$ eV are shown in Fig. 2. The resonant excitation of the 2p state and the subsequent ionization occurs if the laser carrier frequency is $\omega = 0.375$ a.u., which coincides with the transition frequency between the 1s and 2p states (in the weak field limit). The photon energy corresponding to this frequency is 10.204 eV and the expected kinetic energy of the ejected electrons is $\varepsilon_0 = 0.25$ a.u. $= 6.803$ eV.

In the next section it will be shown that the approximate results obtained using the three-level model, in which the exact values for $|d_\varepsilon|^2$ are replaced by the value of $|d_{\varepsilon_0}|^2$, as it was the case in previous studies [6], are sufficient for a qualitative analysis of spectra. The values of the matrix elements for transitions from the 2p state to continuum s and d states at the energy ε_0 are $d_{\varepsilon_0\mathrm{s}} = (0.1469 - 0.0296\,i)$ a.u. and $d_{\varepsilon_0\mathrm{d}} = (-0.0749 - 0.3717\,i)$ a.u., respectively. These values give $|d_{\varepsilon_0}|^2 = 0.1663$ a.u. and the quotient $|d_{\varepsilon_0\mathrm{s}}|^2/|d_{\varepsilon_0\mathrm{d}}|^2 = 0.1563$ which estimates the relative ratio of s and d-electrons in the photoelectron yield.

3 Results

Using the methods described in the previous section, we analyze the populations of atomic states and photoelectron energy spectra for the two-photon ionization of the hydrogen atom by the laser pulse (2) of the gaussian form

$$g(t) = e^{-t^2/\tau^2} \tag{14}$$

with $\tau = 6$ fs and the carrier frequency $\omega = 0.375$ a.u. which is resonant for the transition $1\mathrm{s} \to 2\mathrm{p}$.

Figure 3 shows the evolution of the populations of atomic states 1s and 2p, calculated for the pulse of peak intensity $I_0 = 25\,\mathrm{TW/cm^2}$ ($I_0 = \mathcal{E}_0^2/(8\pi\alpha)$, $\alpha = 1/137$) for which approximately 1.5 Rabi cycles during the pulses are completed. The populations shown in panel (a) were obtained using the method of time-dependent amplitudes described in Sect. 2.1, i.e. by solving the system of Eq. (5) for the recommended set of amplitudes, while those in panel (b) were obtained applying the three-level model described in Sect. 2.2, i.e. by solving the system of Eq. (11). Beside the populations of the 1s and 2p states, in the panel (a) the populations of the states 2s and 3d are shown, too. The populations of other states are significantly smaller and, for this reason, not shown in the figure. A good agreement between the results for the populations of the states 1s and 2p in the panels (a) and (b), as well as relatively small values for populations of other (non-essential) states, confirm the validity of the three-level model, particularly for describing the electron dynamics in the discrete-state subspace.

Figure 4 shows the final populations of the ground and intermediate states, using $t_{\mathrm{ex}} = 3\tau$ for the gaussian pulse (14), as functions of the peak intensity I_0 in the domain of 0.02–400 $\mathrm{TW/cm^2}$. The values obtained using the computational approaches described in Sects. 2.1 and 2.2 practically coincide and for this reason they are represented in the figure by the same lines. The vertical dashed lines indicate the values of I_0 at which the atom manages to complete an integer number of Rabi cycles during the pulse.

Figure 5 shows the photoelectron energy spectra calculated for the laser peak intensities which are in Fig. 4 indicated by the vertical dashed lines. The spectra

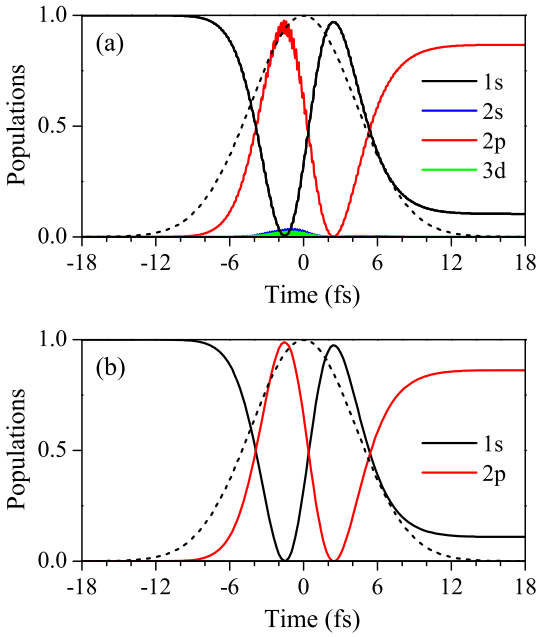

Fig. 3 **a** Populations of the ground state (1s) and the excited states 2s, 2p and 3d of the hydrogen atom during the action of the gaussian laser pulse of 25 TW/cm^2 peak intensity, $\tau = 6$ fs and $\omega = 0.375$ a.u., calculated by solving the set of Eq. (5). **b** Populations of the ground state (1s) and the excited state 2p of the hydrogen atom during the action of the same pulse, calculated by solving the set of Eq. (11) (the three-level model). The dashed line represents the envelope of the laser pulse. For the chosen peak intensity the populations perform approximately 1.5 Rabi cycles during the pulse

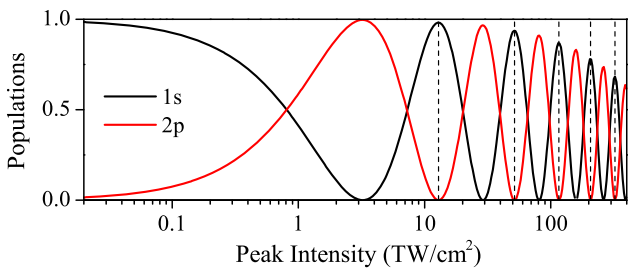

Fig. 4 Populations of the ground (1s) and the excited 2p state of hydrogen, after the laser pulse has expired, as functions of the laser peak intensity. The results are obtained using the gaussian pulse of the carrier frequency $\omega = 0.375$ a.u. (which corresponds to the photon energy of 10.204 eV) and $\tau = 6$ fs. The vertical dashed lines indicate the peak intensities at which an integer number of Rabi cycles is completed during the pulse

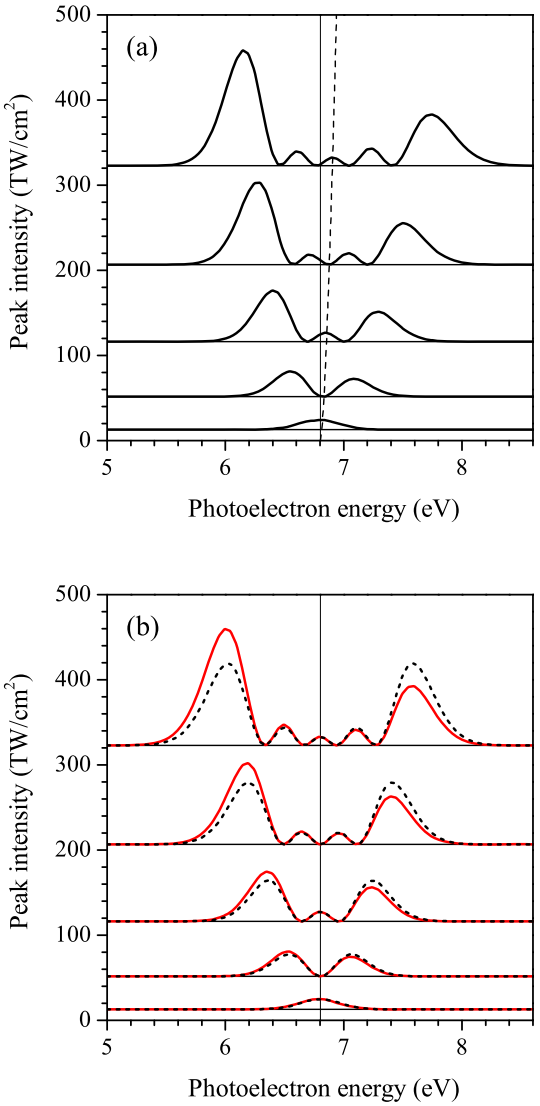

Fig. 5 Calculated photoelectron energy spectra for two-photon ionization of the hydrogen atom by gaussian laser pulses of 6 fs duration, 10.203 eV photon energy, and peak intensities indicated in Fig. 4 by vertical dashed lines. The spectra in panel (**a**) are determined by solving the full set of Eq. (5) with recommended number of states (see the text in Sect. 2.1), while those in panel (**b**) are obtained using the three-level model with exact $|d_\varepsilon|^2$ values (solid red lines) and with $|d_\varepsilon|^2 \approx |d_{\varepsilon_0}|^2$ (dashed lines). The weak field value of the photoelectron energy $\varepsilon_0 = 6.803$ eV is marked by the vertical thin line. The dashed line in panel (**a**) shows the shift of the spectral patterns (AT doublets) which is a slowly increasing function of the laser peak intensity

in panel (a) are determined by solving the system of Eq. (5) and applying Eq. (6), while those in panel (b) are obtained by solving the system of Eq. (11) (the three-level model) and applying Eq. (13) with $|d_\varepsilon|^2$ values shown in Fig. 2 (solid red lines) and, alternatively, with $|d_\varepsilon|^2 \approx |d_{\varepsilon_0}|^2$ (dotted lines). It can be seen that, regardless of the calculation method, for each value of I_0 the spectrum consists of a pattern exhibiting the AT splitting. An exception is the pattern for the laser peak intensity corresponding to one Rabi cycle during the pulse. Namely, the separation between the components of the AT doublet (the edge peaks) is proportional to the field strength [2], and in the one-cycle case this separation is of the same order as the widths of the components.

A notable difference between the spectra shown in panels (a) and (b) of Fig. 5 is a shift of the AT doublets to higher values of the photoelectron energy that exists in the former and does not exist in the latter spectra. The shift increases with the laser peak intensity and can be attributed to the dynamic (AC) Stark shift that is a consequence of coupling of the ground and resonant states with nonessential states [7,8]. Since the last states do not participate in the three-level model, the AC Stark shift is not included and the AT doublets calculated using such an approximate model are not shifted.

Another difference between the spectra obtained using approaches of different degrees of approximation is in the intensity of the AT doublet components. In the spectra obtained using the three-level model with the approximation $|d_\varepsilon|^2 = |d_{\varepsilon_0}|^2$, the edge peaks are of the same intensity, but in the spectra obtained by the method of time-dependent amplitudes with a larger number of states (panel (a)) and those obtained using the three-level model with exact values for $|d_\varepsilon|^2$, the right peak is lower than the left one. According to Refs. [7,8] the AC Stark shift could be an explanation for this kind of asymmetry, too. Namely, the carrier frequency, which is resonant for the transition 1s → 2p, is due to the Stark shift slightly different from the field-free resonant frequency $\omega = 0.375$ a.u., and this detuning may be a reason for the asymmetry [5]. However, our calculations performed within the three-level model with exact values for $|d_\varepsilon|^2$ reproduce very well the asymmetry obtained by the full calculations. Therefore, we conclude that, although the asymmetry in the intensity of the AT doublet components may be partially caused by the AC Stark shift, it is primarily due to the change of the values of matrix elements $d_{\varepsilon l}$ with the photoelectron energy ε.

4 Summary and conclusions

In this paper we analyzed the shift and asymmetry of Autler–Townes doublets observed in the photoelectron energy spectra in the case of two-photon ionization of the hydrogen atom by intense short laser pulses of the carrier frequency which is resonant with the transition 1s → 2p. These doublets are a manifestation of the field induced Rabi flopping of population between the resonantly coupled 1s and 2p (essential) states, but also they carry information about other atomic (nonessential) states and transitions to continuum states. The spectra were calculated applying the method of time-dependent amplitudes using two approaches of different level of approximation. The first approach involves solving a complete set of equations for amplitudes, which, apart from the amplitudes of essential and continuum states, also include the amplitudes of non-essential states. The second approach is the three-level model that includes only the amplitudes of the two essential states (1s, 2p) and those of continuum states. Thus, the AC Stark shift which is a consequence of the coupling of essential states with non-essential ones, can appear only in spectra obtained using the first approach, which was confirmed by the calculations. The asymmetry in the intensity of the Autler–Townes doublet components appears both in the results obtained by the first approach and in the results obtained using the three-level model with exact values of the dipole matrix elements for transitions between the 2p and continuum states. Thus, we conclude that this asymmetry is primarily a consequence of the decrease in the probability of transitions between the 2p and continuum states with increasing photoelectron energy.

Acknowledgements This work was supported by Ministry of Education, Science and Technological Development of Republic of Serbia and by the COST Action No. CM18222 (AttoChem).

Author contributions

All authors contributed to the study conception, material preparation, data collection and its analysis. The first draft of the manuscript was written by the corresponding author (N.S.S). All authors read and approved the final manuscript.

Data Availability Statement This manuscript has no associated data or the data will not be deposited. [Author's comment: The datasets generated during and/or analysed during the current study are available from the corresponding author on reasonable request.]

Appendix A: Matrix elements for dipole transitions

The matrix elements that occur in Eqs. (4), (5) and (8) are conveniently calculated using the coordinate representation for the discrete and continuum energy eigenstates of the bare atom

$$|nl\rangle \to \psi_{nl}(\mathbf{r}) = \mathrm{R}_{nl}(r)\mathrm{Y}_{l0}(\Omega), \tag{15}$$

$$|\varepsilon l\rangle \to \psi_{\varepsilon l}(\mathbf{r}) = \sqrt{\frac{2}{\pi k}}\, i^l e^{-i\sigma_l(k)} \frac{\mathrm{F}_l(\eta, kr)}{r} \mathrm{Y}_{l0}(\Omega), \tag{16}$$

where $\mathrm{R}_{nl}(r)$ and $\mathrm{Y}_{l0}(\Omega)$ are the radial wave functions of hydrogen and the spherical harmonics with $m = 0$, respectively, whereas $\sigma_l = \arg\Gamma(l+1+i\eta)$ and $\mathrm{F}_l(\eta, kr)$ are the Coulomb phase shift and the regular Coulomb functions [15], where $\eta = -1/k$ and $k = \sqrt{2\varepsilon}$ (in atomic units). Then

$$\langle nl|z|n'l'\rangle = \int \psi^*_{nl}(\mathbf{r})\, r\cos\vartheta\, \psi_{n'l'}(\mathbf{r})\, \mathrm{d}^3\mathbf{r} = I^{(\mathrm{dis})}_{nl,n'l'} J_{ll'}, \tag{17}$$

$$\langle nl|z|\varepsilon l'\rangle = \int \psi^*_{nl}(\mathbf{r})\, r\cos\vartheta\, \psi_{\varepsilon l'}(\mathbf{r})\,\mathrm{d}^3\mathbf{r} = \sqrt{\frac{2}{\pi k}}\, i^{l'} e^{-i\sigma_{l'}(k)} I^{(\mathrm{cont})}_{nl,\varepsilon l'} J_{ll'}, \quad (18)$$

where

$$I^{(\mathrm{dis})}_{nl,n'l'} = \int_0^\infty \mathrm{R}_{nl}(r)\,\mathrm{R}_{n'l'}(r)\, r^3\mathrm{d}r, \quad (19)$$

$$I^{(\mathrm{cont})}_{nl,\varepsilon l'} = \int_0^\infty \mathrm{R}_{nl}(r)\,\mathrm{F}_{l'}(\eta,kr)\, r^2\mathrm{d}r, \quad (20)$$

$$J_{ll'} = \int_\Omega \mathrm{Y}_{l0}(\Omega)\,\mathrm{Y}_{l'0}(\Omega)\cos\vartheta\,\mathrm{d}\Omega. \quad (21)$$

References

1. D.A. Steck, Quantum and Atom Optics, http://steck.us/teaching. Accessed 24 Sept 2020 (revision 0.13.4)
2. S.H. Autler, C.H. Townes, Phys. Rev. **100**, 703 (1955)
3. K.J. LaGattuta, Phys. Rev. A **47**, 1560–1563 (1993)
4. M.G. Girju, K. Hristov, O. Kidun, D. Bauer, J. Phys. B **40**, 4165 (2007)
5. D. Rogus, M. Lewenstein, J. Phys. B **19**, 3051 (1986)
6. P.V. Demekhin, L.S. Cederbaum, Phys. Rev. A **86**, 063412 (2012)
7. A.D. Müller, E. Kutscher, A.N. Artemyev, L.S. Cederbaum, P.V. Demekhin, Chem. Phys. **509**, 145 (2018)
8. A. Tóth, A. Csehi, J. Phys. B: At. Mol. Opt. Phys. **54**, 035005 (2021)
9. S. Nandi, E. Olofsson, M. Bertolino, S. Carlström, F. Zapata, D. Busto, C. Callegari, M. Di Fraia, P. Eng-Johnsson, R. Feifel, G. Gallician, M. Gisselbrecht, S. Maclot, L. Neoričić, J. Peschel, O. Plekan, K.C. Prince, R.J. Squibb, S. Zhong, P.V. Demekhin, M. Meyer, C. Miron, L. Badano, M.B. Danailov, L. Giannessi, M. Manfredda, F. Sottocorona, M. Zangrando, J.M. Dahlström, Nature **608**, 488 (2022)
10. M. Baghery, U. Saalmann, J.M. Rost, Phys. Rev. Lett. **118**, 143202 (2017)
11. W.C. Jiang, J. Burgdörfer, Opt. Express **26**, 19921 (2018)
12. N.S. Simonović, D.B. Popović, A. Bunjac, To be published
13. P.V. Demekhin, L.S. Cederbaum, Phys. Rev. A **83**, 023422 (2011)
14. P.V. Demekhin, L.S. Cederbaum, Phys. Rev. A **88**, 043414 (2013)
15. A.R. Barnett, in *Computational Atomic Physics, Electron and Positron Collisions with Atoms and Ions*, ed. by K. Bartschat (Springer, Berlin, 1996), pp.181–202